Beamforming of ultrasound images modelled as stable random variables

Teodora Szasz, Adrian Basarab, Denis Kouamé

Beamforming of ultrasound images modelled as stable random variables

Teodora Szasz, Adrian Basarab, and Denis Kouamé

***Abstract*—This paper presents a new beamforming method for ultrasound medical imaging based upon the statistical characterization of the ultrasound signals by α-stable distributions. The proposed method was evaluated on ultrasound simulated and *in vivo* thyroid data. In simulation, an improvement in contrast ratio of 2.84 dB, 11.52 dB, and 13.33 dB was obtained compared with minimum variance, delay-and-sum, and least squares beamformers respectively. Applied on *in vivo* data and compared to delay-and-sum and least squares, our method increases the contrast ratio between the tumor and the healthy tissue by 1.28 dB, respectively 1.54 dB.**

***Index Terms*—medical ultrasound, beamforming, α-stable statistical distribution, ℓ_p-norm regularization.**

I. Introduction

Beamforming (BF) techniques play a major role in the quality of the US images. The most commonly used BF method is the classical delay-and-sum (DAS) (e.g., [1]). DAS BF consists firstly in focusing the raw channel data received by the elements of the US probe to compensate the delays due to the time-of-flight differences. Then the resulting signals are weighted and further summed up to form one RF signal. The applied weights form the apodization window in reception. Despite its benefits related to its real-time capabilities, DAS BF provides low spatial resolution and contrast. To improve the resolution and the contrast of US images, multiple approaches were developed by adaptively estimating the apodization windows using the raw channel data. These techniques are trying to obtain a minimum variance (MV) beamformer based on the estimated covariance matrix. In US imaging, this type of BF methods is facing two main problems: the first, related to the poor conditioning of the covariance matrix and the second, related to the broadband nature of the raw signals. To overcome these issues, several approaches have been proposed, such as diagonal loading (e.g. [2]), spatial or frequency smoothing of the covariance matrices [3], or iterative methods [4].

In [5] we have reformulated BF in US imaging as a linear inverse problem, associating the raw channel data to the RF signals to be recovered. Numerical optimization routines have been employed to invert the resulting linear model based on standard regularization terms such as ℓ_1-norm, ℓ_2-norm, and elastic net [6]. While US signal processing has widely relied for many years on the assumption of Gaussianity [7], the authors in [8] were the first to show that RF echoes can be more accurately modelled by a power-law shot noise model. Later, this result has been confirmed by other research groups. For example, the statistical properties of the RF signals were related, based on the generalized central limit theorem, to α-stable distributions [9].

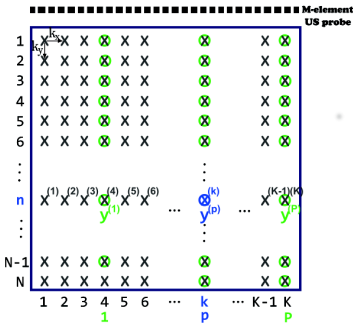

Fig. 1. Main elements used to describe the proposed BF model.

In this paper we propose to take into account the non-Gaussianity properties of the RF signals in the BF process (see e.g., [9]). To the best of our knowledge, this is the first attempt of specifically consider an α-stable distribution while beamforming the received echoes in US imaging. Thus, the direct linear model proposed in [5] is herein inverted using a more general ℓ_p pseudo norm regularization, with p automatically related to the parameter α estimated from the data [10]. Given that p may take values smaller than 1, the resulting non-convex objective function was minimized in this work by the half-quadratic optimization algorithm [11].

II. Acquisition setup

Fig. 1 presents the main elements used to derive the direct model on which is based the proposed BF method.

We consider, without loss of generality, an M-element US probe that is sequentially transmitting P US beams. The beams can be focused, divergent, or plane waves. The reflected echoes are recorded with the same US probe and are time-delayed, so that time-of-flight differences are compensated. Depending on the exploration depth and on the sampling frequency, each recorded signal, after delay compensation (i.e., focalization), has N time samples. Henceforth, unless otherwise specified, all the developments are done for a given depth n (or sample n of the received signal, see Fig. 1), with $n = 1, \cdots, N$.

For each emission $p = 1, \cdots, P$, we consider that M_p elements ($1 \leq M_p \leq M$) are receiving the echoes. Note that in the case when all elements of the US probe are active in reception, $M_1 = M_2 = \cdots = M_p = M$. Let us denote by $\boldsymbol{y}_p \in \mathbb{C}^{M_p \times 1}$ the raw channel data received by the M_p sensors, corresponding to depth n. In this situation, the classical DAS BF can be expressed as:

$$\boldsymbol{y}^{(p)} = \frac{\sum_{i=1}^{M_p} w_i y_p^{(i)}}{\sum_{i=1}^{M_p} w_i}, \tag{1}$$

where $y_p^{(i)}$ is the i^{th} element signal of $\boldsymbol{y}_p$, w_i are fixed BF weights (e.g., Hanning or Hamming windows) and $\boldsymbol{y}^{(p)}$ is the DAS BF signal of the p^{th} emission corresponding to the p^{th} element of vector, $\boldsymbol{y} \in \mathbb{C}^{P\times 1}$. Note that we consider in (1) the standard case, where the horizontal (lateral) grid density of the DAS BF image corresponds to the number of US emissions. In other words, the data received for one emission serves at beamforming one position in the scanning grid. The positions to be beamformed with our method are highlighted by the symbol x and the positions corresponding to DAS BF are drawn by the symbol ◯ in Fig. 1. As we will explain in the next section, the proposed BF method will consider a further laterally refined scanning grid, as shown by the x symbols in Fig. 1.

III. Beamforming of US images modelled as stable random variables

A. Signal model

Let us denote by $\boldsymbol{x}$ the signal at depth n to be beamformed with the proposed method. We denote by K the size of this vector ($K \geq P$) as schematically highlighted in Fig. 1. Note that the total number of sensors M, the number of emissions P, and the number of lateral positions, K, on the scanned grid employed by the proposed method, are independent of each other. For a given depth n, the model relating the received signal (raw channel data) $\boldsymbol{y}_p \in \mathbb{C}^{M_p\times 1}$ to the desired signal $\boldsymbol{x}$ can be written as follows [5]:

$$\boldsymbol{y}_p = (\boldsymbol{A}_p^H \boldsymbol{A}_T)\boldsymbol{x} + \boldsymbol{g}_p, \tag{2}$$

where $\boldsymbol{A}_p \in \mathbb{C}^{M\times M_p}$ and $\boldsymbol{A}_T \in \mathbb{C}^{M\times K}$ are standard steering matrices relating the US probe element positions to the lateral positions on the scanline. More precisely, the form of $\boldsymbol{A}_p$ is considering that the K reflectors to be beamformed are impinging on M_p elements through their reflected pulses, while $\boldsymbol{A}_T$ is relating the positions of the M elements to the K reflectors, under the assumption that the elements are impinging on the reflectors. We denoted by $\boldsymbol{g}_p$ the additive white Gaussian noise affecting the raw channel data and with $(\cdot)^H$ the conjugate transpose. In the following, without loss of generality, we will consider that all US probe elements are active in reception, i.e., $\boldsymbol{A}_1 = \boldsymbol{A}_2 = \cdots = \boldsymbol{A}_p = \boldsymbol{A}$.

To reduce the dimensionality of the raw channel data, we applied beamspace processing [12], a common tool in array processing. It has been shown that in addition to reducing computational complexity sensitivity, beamspace processing allows improving the signal-to-noise ratio (SNR) [13]. Thus, while DAS only beamforms one position on the scanline for each emission, $\boldsymbol{y}_p \in \mathbb{C}^{M_p\times 1}$ in (2) becomes a scalar after applying DAS BF. Finally, arranging all these scalars in a vector denoted by $\boldsymbol{y} \in \mathbb{C}^{P\times 1}$, the system of equations in (2) becomes:

$$\boldsymbol{y} = (\boldsymbol{A}^H \boldsymbol{A}_T)\boldsymbol{x} + \boldsymbol{g}, \tag{3}$$

where $\boldsymbol{A}_T \in \mathbb{C}^{M\times K}$, $\boldsymbol{A} \in \mathbb{C}^{M\times P}$, $\boldsymbol{x} \in \mathbb{C}^{K\times 1}$, and $\boldsymbol{g} \in \mathbb{C}^{K\times 1}$ have the same definition as in (2).

In the following, let us denote $\boldsymbol{\Phi} = \boldsymbol{A}^H \boldsymbol{A}_T$, $\boldsymbol{\Phi} \in \mathbb{C}^{P\times K}$. Thus, the direct model considered by our BF process becomes:

$$\boldsymbol{y} = \boldsymbol{\Phi}\boldsymbol{x} + \boldsymbol{g}. \tag{4}$$

Note that the system to invert is underdetermined, and more generally the inverse problem to solve is ill-posed, thus requiring regularization in order to obtain a valid solution.

B. α-stable distributions model

As explained previously, our BF solution is based on the hypothesis of α-stable distributed US signals. We remind that the characteristic function of a symmetric α-stable ($S\alpha S$) distribution has the form:

$$E(\theta) = \exp\left(j\theta\delta - \gamma|\theta|^\alpha\right), \tag{5}$$

where $\alpha \in (0, 2]$ is the characteristic index, $\delta \in (-\infty, \infty)$ is the location parameter, and $\gamma \in \mathbb{R}^+$ is the spread of the distribution. We emphasize that the stable law is a generalization of the Gaussian distribution, thus for $\alpha = 2$ the stable distribution is reduced to the Gaussian distribution.

Interestingly, due to the stability property of this distribution and to the linear model that relates $\boldsymbol{x}$ to $\boldsymbol{y}$ (4), we can conclude that if $\boldsymbol{x}$ is supposed to follow an $S\alpha S$, then $\boldsymbol{y}$ can also be modelled by an $S\alpha S$ with the same parameter α [10]. This observation has an important practical interest, allowing us to estimate the parameter α corresponding to $\boldsymbol{x}$ from the observed vector $\boldsymbol{y}$. In this work, we have used the method in [14] to estimate the parameter α from the discrete measurements $\boldsymbol{y}$.

C. Model inversion via ℓ_p-norm regularization

We have recently shown, in a different application context (compressive sampling), that the ℓ_p-norm regularization is well adapted to reconstruct $S\alpha S$-distributed signals [10]. Moreover, it has been shown that the optimal choice for parameter p is smaller but as close as possible to α [10], typically $p = \alpha - 0.01$. Following, this result, we propose herein to solve the BF problem in (4) by solving the following minimization problem:

$$\hat{\boldsymbol{x}} = \underset{\boldsymbol{x}}{\operatorname{argmin}}(\|\boldsymbol{y} - \boldsymbol{\Phi}\boldsymbol{x}\|_2^2 + \lambda\|\boldsymbol{x}\|_p^p), \tag{6}$$

where λ is the regularization parameter balancing the tradeoff between the fidelity to the data and the regularization term.

Depending on the sparsity degree of the scanned medium, the value of p, directly related to α estimated from $\boldsymbol{y}$ (i.e., $p = \alpha - 0.01$), can take values smaller than 1. In this case, the function (6) to be minimized becomes non-convex. Several solutions to solve such non-convex problems exist in the literature. In this work, we used the half-quadratic optimization algorithm proposed in [11], where a non-quadratic optimization problem is viewed as multiple quadratic problems. The main steps of the proposed BF approach, for a particular depth n, are described in the pseudo-code below:

IV. Results and discussion

To evaluate the proposed BF method (denoted hereafter by α-stable BF), we used both simulated and *in vivo* data. The simulated data contains 3 point reflectors at 50 mm in depth and an anechoic cyst structure of 10 mm radius at 80 mm in depth, embedded in speckle noise typical for US images. The simulated US probe had 64 elements, with the pitch of

Algorithm 1: α-stable beamforming at depth n.

Input: Raw channel data, $\boldsymbol{y}_p \in \mathbb{C}^{M_p \times 1}$.
Output: α-stable beamformed data, $\boldsymbol{x} \in \mathbb{C}^{K \times 1}$.
1) Apply DAS BF to $\boldsymbol{y}_p$ using (1) $\Rightarrow \boldsymbol{y} \in \mathbb{C}^{P \times 1}$.
2) Estimate α from $\boldsymbol{y}$.
3) Calculate p as: $p = \alpha - 0.01$.
4) Solve (6) using half-quadratic optimization $\Rightarrow \hat{\boldsymbol{x}}$.

TABLE I
CR, CNR, AND FWHM VALUES FOR SIMULATED DATA BEAMFORMED IMAGES IN FIG. 2

BF Method	CR[dB]	CNR	FWHM [mm]
DAS	58.22	6.40	1.55
MV	66.90	5.98	0.92
LS	56.41	6.08	1.29
α-stable	**69.74**	**7.65**	**0.32**

256 μm, the height of 5 mm, and the center frequency of 3 MHz. The emissions corresponded to 52 steered plane waves (for the proposed method) and 260 steered plane waves (for DAS/MV BF methods), for angles between -30° and 30°. The raw channel data was obtained using the state-of-the art ultrasound simulator Field II [15].

The *in vivo* data represents the thyroid gland from a subject with a malignant tumor. The acquisition was done with a clinical Sonoline Elegra ultrasound system modified for research purposes, equipped with a Siemens Medical Systems 7.5L40 P/N 5260281-L0850 linear array transducer, emitting series of focalized waves.

Two of the most commonly used image quality metrics were calculated (the contrast-to-noise ratio - CNR and the contrast ratio - CR [dB]). Based on the mean values in a region R_1 (for simulated data it corresponds to a region inside the anechoic cyst structure and for *in vivo* data to a region inside the tumor) and a region R_2 (for both types of data it is a region in the homogeneous surrounding speckle, at the same depth with the region R_1), CR is defined as $CR = |\mu_{R_1} - \mu_{R_2}|$, where μ_{R_1} and μ_{R_2} are the mean values of intensities in region R_1, respectively R_2. CNR is defined as $CNR = \frac{|\mu_{R_1} - \mu_{R_2}|}{\sqrt{\sigma^2_{R_1} + \sigma^2_{R_2}}}$, where σ_{R_1} and σ_{R_2} are the standard deviations of intensities in R_1, respectively R_2. The results of simulated data were compared with standard DAS and MV method in [16]. Moreover, we have also compared our results to those obtained with the same BF model as the one proposed herein, but using a standard Tikhonov regularization (i.e. p equal to 2 in (6)) [17]. This method has been named LS (least-squares) BF. Since the *in vivo* data was acquired with a clinical scanner, the raw channel data necessary to apply MV was not accessible. Thus the results on *in vivo* data were only compared with standard DAS and LS BF methods.

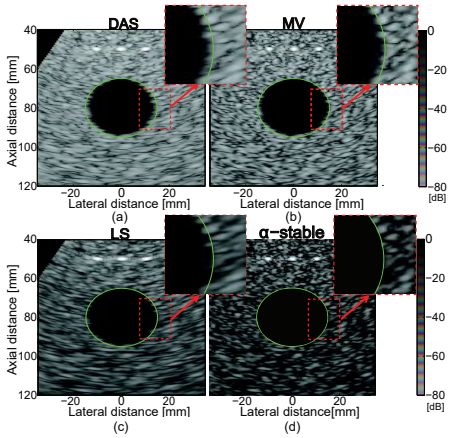

Fig. 2. Results of (a) DAS, (b) MV, (c) LS (Tikhonov), and (d) $\alpha-$stable BF methods on simulated data with point reflectors and an anechoic cyst structure. The image quality metrics: CR, CNR, and FWHM are given in the Table I.

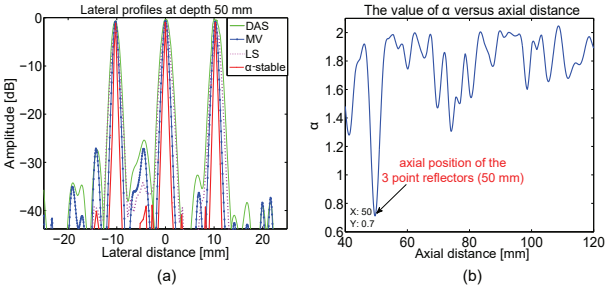

Fig. 3. (a) Lateral profiles at 50 mm of the DAS, MV, LS, and α-stable BF methods in Fig. 2; (b) the value of α versus the axial distance in Fig. 2.

A. Simulated data with point reflectors and an anechoic cyst structure

Fig. 2 presents the BF results of the simulated data containing 3 point reflectors and an hypoechoic cyst. The green circle represents the true border of the cyst. We can observe that DAS BF (Fig. 2(a)) is not able to resolve the dimensionality of the circular cyst. The cyst appears narrower than its original dimension, due to the low resolution provided by DAS. MV (Fig. 2(b)) and LS BF (Fig. 2(c)) provide better resolved results, i.e. the dimension of the cyst is closer to its real dimension. However, when using α-stable BF (Fig. 2(d)) we obtain better result in terms of spatial resolution, contrast, and resolution of the dimensionality of the scanned structures, compared with DAS, MV, and LS. The gain in contrast can be observed in the Table I, where α-stable BF provides an improvement of 11.52 dB compared with DAS and of 2.84 dB compared with MV. Note that DAS and MV used raw channel data resulting from 5 times more US emissions than our method (i.e. 260 plane waves), such as the density of the BF grid was the same for all beamformers.

Fig. 3(a) depicts the lateral profiles at depth 50 mm (passing through the 3 point reflectors) obtained with the aforementioned BF methods. As expected, the 3 points reflectors are better resolved by α-stable beamformer, having narrower mainlobe and lower sidelobes compared with the other BF

TABLE II
CR AND CNR VALUES FOR THE *in vivo* THYROID BEAMFORMED IMAGES IN FIG. 4

BF Method	CR[dB]	CNR
DAS	2.98	0.16
LS	2.72	0.22
α-stable	**4.26**	**0.24**

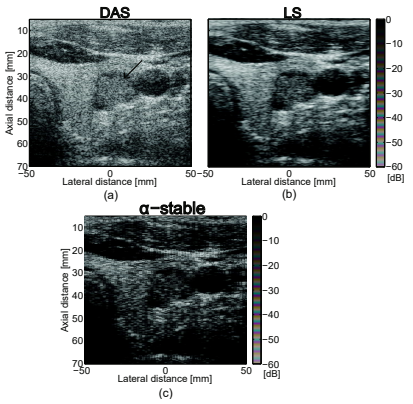

Fig. 4. Results of (a) DAS, (b) LS, and (c) $\alpha-$stable BF methods on *in vivo* data of thyroid with malignant tumor (highlighted by the black arrow). The image quality metrics: CR and CNR are given in the Table II.

methods (we used FWHM - full width at half maximum, in Table I, as quantitative indicator). Fig. 3(b) illustrates the dependence of estimated parameter α on the structures at each depth of image in Fig. 2. We can observe that the minimum value of ($\alpha = 0.7$) is reached at depth 50 mm, where the 3 point reflectors are positioned, imposing sparse conditions to the scanned medium. Moreover, a value of $\alpha \approx 2$ is reached at the depths containing only homogeneous speckle structures, thus following a Gaussian distribution. The ability of α to adapt to the characteristics of the scanned medium is of high interest, as it allows p to automatically adapt to its best value in the optimization process.

B. In vivo data: thyroid with malignant tumor

The results of the BF of the thyroid data with a malignant tumor can be observed in the Fig. 4. The tumor (highlighted by the black arrow in Fig. 4(a)) is located in the left lobe of the thyroid, in the proximity of the carotid artery (the hypoechoic (dark) circular structure). The values of CR and CNR metrics are presented in the Table II. Regarding the detection of the tumor, we can observe that by using DAS BF (Fig. 4(a)) it is difficult to delimit the region of the tumor because of the poor contrast and resolution of the image. The visual detection is improved when using LS BF (Fig. 4(b)). Furthermore, due to the increase in contrast, the edges of the tumor can be better visualized when using α-stable BF (Fig. 4(c)), compared with DAS and LS BF. Note that the raw channel *in vivo* data was not accessible (only DAS RF beamformed image was available), which may explain some banding artifacts visible on the α-stable final image (Fig. 4(c)).

V. CONCLUSION

In this paper, we proposed a new BF method, by generalizing the previously proposed BF model in ultrasound imaging. Our method uses an ℓ_p-norm regularization to solve the inverse problem on which our model is based. Moreover, p is automatically calculated by relating it to the α-stable statistics of US images. Thus, our method, in contrast to minimum variance approaches, does not require any hyperparameter tuning and could also be of interest in other application domains such as direction of arrival estimation. Future work will include the evaluation of other acquisition strategies (e.g., ultrasound emissions in random directions) or the consideration of joint regularization terms for the joint reconstruction of several scanlines.

REFERENCES

[1] K. E. Thomenius, "Evolution of ultrasound beamformers," in *, 1996 IEEE Ultrasonics Symposium, 1996. Proceedings*, Nov. 1996, vol. 2, pp. 1615–1622 vol.2.

[2] B. M. Asl and A. Mahloojifar, "A low-complexity adaptive beamformer for ultrasound imaging using structured covariance matrix," *IEEE Transactions on Ultrasonics, Ferroelectrics, and Frequency Control*, vol. 59, no. 4, pp. 660–667, Apr. 2012.

[3] I. K. Holfort, F. Gran, and J. A. Jensen, "Broadband minimum variance beamforming for ultrasound imaging," *IEEE Transactions on Ultrasonics, Ferroelectrics, and Frequency Control*, vol. 56, no. 2, pp. 314–325, Feb. 2009.

[4] A.C. Jensen and A. Austeng, "The iterative adaptive approach in medical ultrasound imaging," *IEEE Transactions on Ultrasonics, Ferroelectrics, and Frequency Control*, vol. 61, no. 10, pp. 1688–1697, Oct. 2014.

[5] T. Szasz, A. Basarab, and D. Kouamé, "Beamforming through regularized inverse problems in ultrasound medical imaging," *IEEE Transactions on Ultrasonics, Ferroelectrics, and Frequency Control*, 2016.

[6] T. Szasz, A. Basarab, M-F. Vaida, and D. Kouamé, "Elastic-Net Based Beamforming in Medical Ultrasound Imaging," in *2016 IEEE International Symposium on Biomedical Imaging*, 2016.

[7] Robert F. Wagner, Michael F. Insana, and David G. Brown, "Statistical properties of radio-frequency and envelope-detected signals with applications to medical ultrasound," *Journal of the Optical Society of America A*, vol. 4, no. 5, pp. 910, May 1987.

[8] M. A. Kutay, A. P. Petropulu, and C. W. Piccoli, "On modeling biomedical ultrasound RF echoes using a power-law shot-noise model," *IEEE Transactions on Ultrasonics, Ferroelectrics, and Frequency Control*, vol. 48, no. 4, pp. 953–968, July 2001.

[9] M. Pereyra and H. Batatia, "Modeling ultrasound echoes in skin tissues using symmetric α-stable processes," *IEEE Transactions on Ultrasonics, Ferroelectrics, and Frequency Control*, vol. 59, no. 1, pp. 60–72, Jan. 2012.

[10] A. Achim, A. Basarab, G. Tzagkarakis, P. Tsakalides, and D. Kouamé, "Reconstruction of Ultrasound RF Echoes Modeled as Stable Random Variables," *IEEE Transactions on Computational Imaging*, vol. 1, no. 2, pp. 86–95, June 2015.

[11] M. Cetin and W.C. Karl, "Feature-enhanced synthetic aperture radar image formation based on nonquadratic regularization," *IEEE Transactions on Image Processing*, vol. 10, no. 4, pp. 623–631, Apr. 2001.

[12] D. Malioutov, M. Cetin, and A.S. Willsky, "A sparse signal reconstruction perspective for source localization with sensor arrays," *IEEE Transactions on Signal Processing*, vol. 53, no. 8, pp. 3010–3022, Aug. 2005.

[13] M. Tanter and M. Fink, "Ultrafast imaging in biomedical ultrasound," *IEEE Transactions on Ultrasonics, Ferroelectrics, and Frequency Control*, vol. 61, no. 1, pp. 102–119, Jan. 2014.

[14] V. Zolotarev, "Mellin-Stieltjes Transforms in Probability Theory," *Theory of Probability & Its Applications*, vol. 2, no. 4, pp. 433–460, Jan. 1957.

[15] J.A. Jensen, "Simulation of advanced ultrasound systems using Field II," in *IEEE International Symposium on Biomedical Imaging: Nano to Macro, 2004*, Apr. 2004, pp. 636–639 Vol. 1.

[16] B.M. Asl and A. Mahloojifar, "Minimum variance beamforming combined with adaptive coherence weighting applied to medical ultrasound imaging," *IEEE Transactions on Ultrasonics, Ferroelectrics, and Frequency Control*, vol. 56, no. 9, pp. 1923–1931, Sept. 2009.

[17] B. Madore and F. C. Meral, "Reconstruction algorithm for improved ultrasound image quality," *IEEE Transactions on Ultrasonics, Ferroelectrics, and Frequency Control*, vol. 59, no. 2, pp. 217–230, Feb. 2012.